J|A|C|S ARTICLES

Published on Web 11/15/2010

Self-Cross-Linked Polymer Nanogels: A Versatile Nanoscopic Drug Delivery Platform

Ja-Hyoung Ryu, Reuben T. Chacko, Siriporn Jiwpanich, Sean Bickerton, R. Prakash Babu, and S. Thayumanavan*

Department of Chemistry, University of Massachusetts Amherst, Amherst, Massachusetts 01003, United States

Received August 4, 2010; E-mail: thai@chem.umass.edu

Abstract: Nanoscopic vehicles that stably encapsulate drug molecules and release them in response to a specific trigger are of great interest due to implications in therapeutic applications, especially for cancer therapy. For this purpose, we have synthesized highly stable polymeric nanogels, in which the kinetics of guest molecule release can be fine-tuned by control over cross-linking density. The polymer nanogel precursor is based on a random copolymer that contains oligoethyleneglycol (OEG) and pyridyldisulfide (PDS) units as side-chain functionalities. By introducing variations into the precursor polymer, such as molecular weight and the relative percentages of hydrophilic OEG units and hydrophobic PDS functionalities, we have achieved significant control over nanogel size. We show that the noncovalently encapsulated guest molecules can be released in response to a redox trigger, glutathione (GSH). Stability of dye encapsulation inside the nanogels and tunability in the release of guest molecules have been demonstrated through in vitro fluorescence resonance energy transfer (FRET) experiments. We show in vitro doxorubicin delivery into breast cancer cells (MCF-7) with nanogels of different cross-linking density to demonstrate that it plays a key role in the stable encapsulation of hydrophobic drug molecules and the cell-uptake efficiencies.

Introduction

Noncovalently binding hydrophobic guest molecules in a water-soluble container and then releasing them in response to a specific trigger are important goals in supramolecular chemistry, carrying clear implications in applications such as drug delivery.[1] When execution of these supramolecular events is based on a nanosized host, there is even greater interest because of the potential for passive targeting of tumor tissue through the enhanced permeability and retention effect.[2] Designing nanoscale objects as drug carriers, to exploit the enhanced permeation and retention effect, can be broadly classified into two categories: covalent incorporation of drugs onto nanoscale scaffolds and noncovalent sequestration of drugs into nanoscale assemblies. Covalent approaches, which include scaffolds such as polymers,[3] dendrimers,[4] and metallic nanoparticles,[5] have the advantage of precise engineering of the nanoscale structure. Noncovalent approaches, on the other hand, have the advantage of not having to incorporate the drug molecules as prodrugs. Liposomes constitute a promising scaffold capable of stable, noncovalent guest molecule encapsulation. However, this assembly is useful mainly for hydrophilic drug molecules or lipophilic drug molecules that can be temporarily rendered hydrophilic.[6]

Micellar assemblies are arguably the most widely explored supramolecular nanoscale assemblies for noncovalent sequester-

(1) (a) Peer, D.; Karp, J. M.; Hong, S.; Farokhzad, O. C.; Margalit, R.; Langer, R. *Nat. Nanotechnol.* **2007**, *2*, 751–760. (b) Haag, R. *Angew. Chem., Int. Ed.* **2004**, *43*, 278–282. (c) Allen, T. M.; Cullis, P. R. *Science* **2004**, *303*, 1818–1822. (d) Kale, T. S.; Klaikherd, A.; Popere, B.; Thayumanavan, S. *Langmuir* **2009**, *25*, 9660–9670. (e) Koo, O. M.; Rubinstein, I.; Onyuksel, H. *Nanomedicine: NBM* **2005**, *1*, 193–212. (f) Oh, J. K.; Drumright, R.; Siegwart, D. J.; Matyjaszewski, K. *Prog. Polym. Sci.* **2008**, *33*, 448–477. (g) West, K. R.; Otto, S. *Curr. Drug Discovery Technol.* **2005**, *2*, 123–160. (h) Bachelder, E. M.; Beaudette, T. T.; Broaders, K. E.; Dashe, J.; Fréchet, J. M. J. *J. Am. Chem. Soc.* **2008**, *130*, 10494–10495. (i) Lee, C. C.; MacKay, J. A.; Fréchet, J. M. J.; Szoka, F. C. *Nat. Biotechnol.* **2005**, *23*, 1517–1526. (j) Jeong, B.; Bae, Y. H.; Lee, D. S.; Kim, S. W. *Nature* **1997**, *388*, 860–862.

(2) (a) Maeda, H.; Wu, J.; Sawa, T.; Matsumura, Y.; Hori, K. *J. Controlled Release* **2000**, *65*, 271–284. (b) Baban, D. F.; Seymour, L. W. *Adv. Drug Delivery Rev.* **1998**, *34*, 109–119. (c) Duncan, R. *Nat. Rev. Drug Discovery* **2003**, *2*, 347–360. (d) Gillies, E. R.; Fréchet, J. M. J. *Drug Discovery Today* **2005**, *10*, 35–43.

(3) (a) Duncan, R. *Nat. Rev. Cancer* **2006**, *6*, 688–701. (b) Greco, F.; Vicent, M. J. *Adv. Drug Delivery Rev.* **2009**, *61*, 1203–1213. (c) MacKay, J. A.; Chen, M.; McDaniel, J. R.; Liu, W.; Simnick, A. J.; Chilkoti, A. *Nat. Mater.* **2009**, *8*, 993–999. (d) Mrkvan, T.; Sirova, M.; Etrych, T.; Chytil, P.; Strohalm, J.; Plocova, D.; Ulbrich, K.; Rihova, B. *J. Controlled Release* **2005**, *110*, 119–129. (e) Miller, K.; Erez, R.; Segal, E.; Shabat, D.; Satchi-Fainaro, R. *Angew. Chem., Int. Ed.* **2009**, *48*, 2949–2954.

(4) (a) Fox, M. E.; Guillaudeu, S.; Fréchet, J. M. J.; Jerger, K.; Macaraeg, N.; Szoka, F. C. *Mol. Pharmaceutics* **2009**, *6*, 1562–1572. (b) Patri, A. K.; Kukowska-Latallo, J. F.; Baker, J. R. *Adv. Drug Delivery Rev.* **2005**, *57*, 2203–2214. (c) van der Poll, D. G.; Kieler-Ferguson, H. M.; Floyd, W. C.; Guillaudeu, S. J.; Jerger, K.; Szoka, F. C.; Fréchet, J. M. J. *Bioconjugate Chem.* **2010**, *21*, 764–773. (d) Choi, S. K.; Thomas, T.; Li, M.-H.; Kotlyar, A.; Desai, A.; Baker, J. R. *Chem. Commun.* **2010**, 2632–2634. (e) Ihre, H. R.; Padilla De Jesús, O. L.; Szoka, F. C.; Fréchet, J. M. J. *Bioconjugate Chem.* **2002**, *13*, 443–452. (f) Lee, C. C.; Gillies, E. R.; Fox, M. E.; Guillaudeu, S. J.; Fréchet, J. M. J.; Dy, E. E.; Szoka, F. C. *Proc. Natl. Acad. Sci. U.S.A.* **2006**, *103*, 16649–16654.

(5) (a) Kim, C. K.; Ghosh, P.; Rotello, V. M. *Nanoscale* **2009**, *1*, 61–67. (b) Agasti, S. S.; Chompoosor, A.; You, C. C.; Ghosh, P.; Kim, C. K.; Rotello, V. M. *J. Am. Chem. Soc.* **2009**, *131*, 5728.

ing of hydrophobic guest molecules in aqueous solution.[2c,7] However, micellar assemblies formed from small molecule surfactants have inherent stability issues. While the assemblies formed from amphiphilic polymers tend to exhibit enhanced stability,[8] these still face certain complications. First, the critical concentration required for assembly formation limits the practicality of in vivo micelle utilization, as large dilution is likely to occur during biodistribution, causing undesirable release of the encapsulated drug payload before arrival at the target site.[9] Second, the interactions between micelles and biological components, such as cellular membranes and blood components, can lead to release of the cargo from the micelle core at undesirable locations.[10] Finally, it has been shown recently that the encapsulation stability of these systems in aqueous solution is relatively poor.[11] We have recently communicated our preliminary findings on chemically cross-linked nanogel systems that can noncovalently encapsulate lipophilic guest molecules.[12] We elaborate the details of our preliminary findings and have included additional details in this Article, such as size control and evaluation of these nanogels as potential drug delivery vehicles.

A versatile drug delivery vehicle should exhibit a few key characteristics: (i) the delivery vehicle should have a desirable and tunable particle size for the enhanced permeability and retention effect; (ii) lipophilic drug molecules should be easily incorporated noncovalently within these nanoparticles; (iii) carrier and encapsulation stability should prevent premature drug release before approaching the target site; (iv) payload release should be triggered by external stimuli in the target cell environment; (v) the release kinetics should be tunable; (vi) the delivery vehicle should not exhibit inherent toxicity; and (vii) synthetic methods of the delivery vehicle should be reliable and reproducible. With these as the defining criteria, we have evaluated our nanogels, and the details of these evaluations are presented here.

Results and Discussion

Design, Syntheses, and the Size Control of the Nanogels. Chemically cross-linked-nanogels are promising scaffolds for satisfying the criteria mentioned above.[13] Nanogels are generally prepared by microemulsion or inverse microemulsion methods.[1h,14] Microemulsion methods, which involve oil-in-water emulsion, utilize lipophilic monomers to produce the nanogels, which are thus generally water insoluble. On the other hand, inverse microemulsion methods do produce water-soluble nanogels. However, because of the synthetic environment, using the water-in-oil-based microemulsion method to encapsulate hydrophobic drugs during gel formation is difficult. Moreover, these methods are relatively complex and require multiple purification steps to remove unreacted monomers and surfactants that are used as emulsion stabilizers. Conversely, the formation of nanoparticles or nanogels from linear polymers by intra-/interchain collapse can be a facile method to make well-defined, biocompatible delivery vehicles.[15] However, these methods require high dilution conditions and thus can be limiting in terms of the extent of guest encapsulation. The nanogel formation method used here circumvents these issues, providing water-soluble nanogels with high lipophilic encapsulation capabilities.

To obtain polymer nanogels with the characteristics mentioned above, it is desirable that (i) we incorporate a functional group that specifically responds to a biologically relevant stimulus; (ii) the syntheses are achieved in the aqueous phase from a water-soluble precursor polymer; and (iii) noncovalent encapsulation of hydrophobic guest molecules is achieved under mild conditions. We envisioned a polymer nanoparticle that is cross-linked with disulfide bonds, where the kinetics of drug release would be controlled by the degree of cross-linking. Also, because gel formation is accomplished by a simple thiol−disulfide exchange, the reaction conditions are mild and do not require the use of organic solvents, metal-containing catalysts, or additional reagents.

Structures of the nanogel precursors, polymer nanogels, and synthetic approach are shown in Figure 1. The polymer nanogel precursor is based on a random copolymer that contains oligoethyleneglycol (OEG) units and pyridyldisulfide (PDS) groups as side chain functionalities. Polymers (**1**−**4**) were prepared by reversible addition−fragmentation chain transfer (RAFT) polymerization. The role of the OEG unit is to introduce a charge-neutral hydrophilic functional group, which is known to endow biocompatibility. The PDS functionality plays several key roles: (i) this is a lipophilic functionality and thus plays a critical role in providing a supramolecular amphiphilic nanoassembly in the aqueous phase. Note that this feature avoids the use of any additional surfactant molecules to generate the nanogel, and the size of this nanoassembly dictates the size of the final polymer nanogel. (ii) The amphiphilic nature of the assembly and lipophilic environment afforded by the PDS functionality provides the opportunity for lipophilic guest molecules to be sequestered within these nanoassemblies prior to cross-linking. (iii) The PDS functionality is reactive, but specific, to thiols and thus provides a mild method for disulfide cross-linking to form the nanogel. (iv) Because the nanogels are based on disulfide cross-linkers that can be cleaved by

(6) (a) Abu Lila, A. S.; Ishida, T.; Kiwada, H. *Expert Opin. Drug Delivery* **2009**, *6*, 1297–1309. (b) Eliaz, R. E.; Nir, S.; Marty, C.; Szoka, F. C. *Cancer Res.* **2004**, *64*, 711–718. (c) Andresen, T. L.; Jensen, S. S.; Jorgensen, K. *Prog. Lipid Res.* **2005**, *44*, 68–97. (d) Torchilin, V. P. *Nat. Rev. Drug Discovery* **2005**, *4*, 145–160.

(7) (a) Liu, S.; Maheshwari, R.; Kiick, K. L. *Macromolecules* **2009**, *42*, 3–13. (b) Davis, M. E.; Chen, Z.; Shin, D. M. *Nat. Rev. Drug Discovery* **2008**, *7*, 771–782. (c) Kataoka, K.; Harada, A.; Nagasaki, Y. *Adv. Drug Delivery Rev.* **2001**, *47*, 113–131. (d) Savić, R.; Luo, L.; Eisenberg, A.; Maysinger, D. *Science* **2003**, *300*, 615–618. (e) Yoo, H. S.; Park, T. G. *J. Controlled Release* **2004**, *96*, 273–283. (f) Yin, H.; Bae, Y. H. *J. Controlled Release* **2008**, *131*, 2–4.

(8) (a) Lavasanifar, A.; Samuel, J.; Kwon, G. S. *Adv. Drug Delivery Rev.* **2002**, *54*, 169–190. (b) Gaucher, G.; Dufresne, M. H.; Sant, V. P.; Kang, N.; Maysinger, D.; Leroux, J. C. *J. Controlled Release* **2005**, *109*, 169–188. (c) Kataoka, K.; Harada, A.; Nagasaki, Y. *Adv. Drug Delivery Rev.* **2001**, *47*, 113–131.

(9) Bae, Y. H.; Yin, H. *J. Controlled Release* **2008**, *131*, 2–4.

(10) (a) Chen, H.; Kim, S.; Li, L.; Wang, S.; Park, K.; Cheng, J.-X. *Proc. Natl. Acad. Sci. U.S.A.* **2008**, *105*, 6596–6601. (b) Chen, H.; Kim, S.; He, W.; Wang, H.; Low, P. S.; Park, K.; Cheng, J.-X. *Langmuir* **2008**, *24*, 5213–5217. (c) Xu, P.; Gullotti, E.; Tong, L.; Highley, C. B.; Errabelli, D. R.; Hasan, T.; Cheng, J.-X.; Kohane, D. S.; Yeo, Y. *Mol. Pharmaceutics* **2009**, *6*, 190–201.

(11) Jiwpanich, S.; Ryu, J.-H.; Bickerton, S.; Thayumanavan, S. *J. Am. Chem. Soc.* **2010**, *132*, 10683–10685.

(12) Ryu, J.-H.; Jiwpanich, S.; Chacko, R.; Bickerton, S.; Thayumanavan, S. *J. Am. Chem. Soc.* **2010**, *132*, 8246–8247.

(13) (a) Kabanov, A. V.; Vinogradov, S. V. *Angew. Chem., Int. Ed.* **2009**, *48*, 5418–5429. (b) Raemdonck, K.; Demeester, J.; Smedt, S. D. *Soft Matter* **2009**, *5*, 707–715.

(14) (a) Sisson, A. L.; Steinhilber, D.; Rossow, T.; Welker, P.; Licha, K.; Haag, R. *Angew. Chem., Int. Ed.* **2009**, *48*, 7540–7545. (b) Oh, J. K.; Siegwart, D. J.; Lee, H.-i.; Sherwood, G.; Peteanu, L.; Hollinger, J. O.; Kataoka, K.; Matyjaszewski, K. *J. Am. Chem. Soc.* **2007**, *129*, 5939–5945.

(15) (a) Kadlubowski, S.; Grobelny, J.; Olejniczak, W.; Cichomski, M.; Ulanski, P. *Macromolecules* **2003**, *36*, 2484–2492. (b) Jiang, J.; Thayumanavan, S. *Macromolecules* **2005**, *38*, 5886–5891. (c) Mackay, M. E.; Dao, T. T.; Tuteja, A.; Ho, D. L.; Horn, B. V.; Kim, H.-C.; Hawker, C. J. *Nat. Mater.* **2003**, *2*, 762–766. (d) Cherian, A. E.; Sun, F. C.; Sheiko, S. S.; Coates, G. W. *J. Am. Chem. Soc.* **2007**, *129*, 11350–11351.

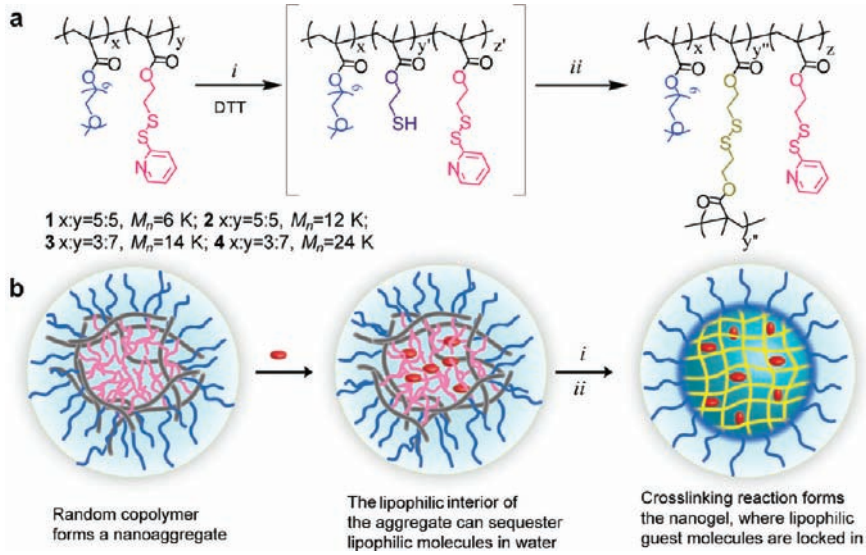

Figure 1. (a) Structure of the polymer precursors and nanogels: (i) cleavage of specific amount of PDS group by DTT, and (ii) nanogel formation by inter/intrachain cross-linking. (b) Schematic representation of the preparation of the biodegradable nanogels.

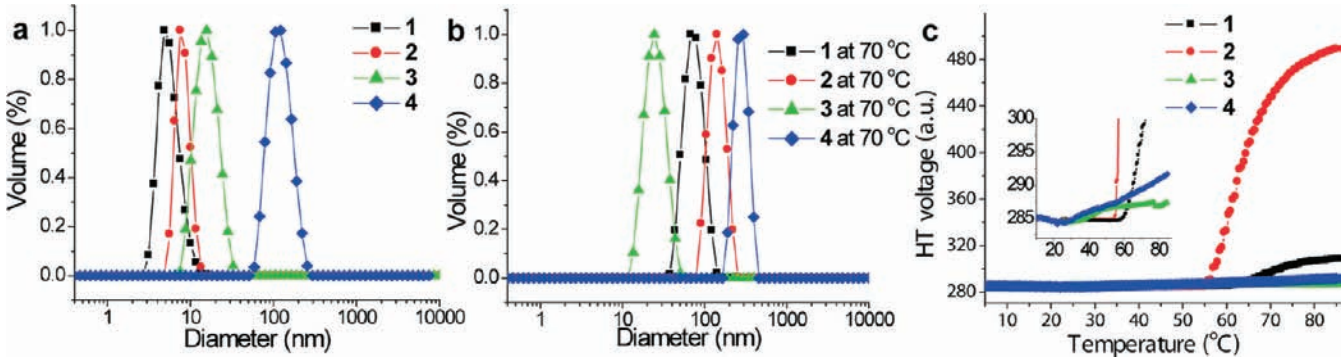

Figure 2. Size distribution of the polymer aggregates at (a) 25 °C and (b) 70 °C in water. (c) Turbidity experiment showing the change in high tension voltage with temperature of the polymer (inset: magnification shows subtle changes in high tension voltage in polymers **3** and **4**).

thiol−disulfide exchange reactions, these nanogels also have a pathway to release the stably encapsulated guest molecules.

We prepared four polymers that have different molecular weights and different ratios of the OEG units to the PDS groups. Polymers **1** (M_n, 6000; PDI, 1.2) and **2** (M_n, 12 000; PDI, 1.2) contain 50% of the OEG methacrylate and 50% of the PDS-derived methacrylate. Polymers **3** (M_n, 14 000; PDI, 1.6) and **4** (M_n, 24 000; PDI, 1.6) consist of 30% of the OEG methacrylate and 70% of the PDS-derived methacrylate. We investigated the aggregate sizes of the polymers in the aqueous phase by dynamic light scattering (DLS), as it was hypothesized that the sizes of these nanoassemblies would dictate the sizes of the obtained nanogels. Polymers **1**, **2**, **3**, and **4** (1 wt %) showed assemblies of 5, 8, 12, and 120 nm diameter in water, respectively (Figure 2a). Interestingly, the polymers showed larger aggregates at high temperature, presumably because of the lower critical solution temperature (LCST) behavior of the OEG units (Figure 2b).[16] The degree of hydration of multiple OEG side chains reduces with increasing temperature, resulting in a compact coil conformation and the polymer becomes more hydrophobic. This leads to intermolecular associations between the polymers, resulting in the formation of larger aggregates.[17]

The LCST behavior of the polymers was investigated by temperature-dependent turbidity measurements using circular dichroism. The polymer (10 mg/mL) solutions were prepared, and the changes in the high tension voltage were monitored at 600 nm by varying the temperature by 2 °C/min.[18] As shown in Figure 2c, polymers **1** and **2** showed large turbidity change above 60 and 55 °C, while polymers **3** and **4** showed a small change above 30 and 25 °C, respectively. This observation is attributed to the fact that the hydrophobicity in the polymer affects the LCST behavior.[19] At the same comonomer composition, the turbidity change and the size are larger with increasing molecular weight due to the cooperative effect of the larger amount of OEG units.[19] The polymer aggregates formed using these LCST behaviors are summarized in Table 1.

The next step involves the conversion of these polymeric aggregates into chemically cross-linked nanogels. We had

(16) (a) Saeki, S.; Kuwahara, N.; Nakata, M.; Kaneko, M. *Polymer* **1976**, *17*, 685–689. (b) Lutz, J.-F.; Akdemir, Ö.; Hoth, A. *J. Am. Chem. Soc.* **2006**, *128*, 13046–13047. (c) Lutz, J.-F.; Weichenhan, K.; Akdemir, Ö.; Hoth, A. *Macromolecules* **2007**, *40*, 2503–2508. (d) Aathimanikandan, S. V.; Savariar, E. N.; Thayumanavan, S. *J. Am. Chem. Soc.* **2005**, *127*, 14922–14929.

(17) Vo, C. D.; Kuckling, D.; Adler, H.-J. P.; Schönhoff, M. *Colloid Polym. Sci.* **2002**, *280*, 400–409.

(18) Klaikherd, A.; Nagamani, C.; Thayumanavan, S. *J. Am. Chem. Soc.* **2009**, *131*, 4830–4838.

(19) Wang, Y.-C.; Li, Y.; Yang, X.-Z.; Yuan, Y.-Y.; Yan, L.-F.; Wang, J. *Macromolecules* **2009**, *42*, 3026–3032.

Table 1. Properties of Polymers and the Sizes of the Polymer Aggregates and Nanogels

polymer	M_n (PDI)[a]	comonomer composition (OEG:PDS)[b]	aggregate size (nm)[c] 25 °C	aggregate size (nm)[c] 70 °C	nanogel size (nm) (PDI)
1	6900 (1.2)	47:53	5	74	68 (0.07)[d]
2	13 100 (1.2)	50:50	8	142	106 (0.03)[d]
3	14 400 (1.6)	33:67	12	24	26 (0.24),[d] 10 (0.33)[e]
4	24 700 (1.6)	31:69	120	255	190 (0.24)[e]

[a] Estimated by GPC (THF) using PMMA standard. [b] Determined by NMR. [c] Determined by DLS. [d] Prepared at 70 °C. [e] Prepared at 25 °C.

hypothesized the formation of the nanogel through the following process. Addition of a deficient amount of dithiothreitol (DTT) would cause the cleavage of a well-defined percentage of the PDS groups to the corresponding thiol functionalities. These thiol functionalities will then react within the polymeric aggregates with unreacted PDS functionalities. This reaction results in disulfide cross-links within the polymeric aggregates, causing the formation of the nanogels, as shown in Figure 1.

By the addition of a deficient amount of DTT into these polymer assembly solutions, we were indeed able to achieve precise control of the size of the cross-linked nanoparticles from ~10 nm to ~200 nm in diameter. To cross-link the polymer aggregates at different temperatures, we added 20 mol % of DTT against total PDS groups in each polymer. We characterized the structures obtained from these reactions by transmission electron microscopy (TEM) and DLS. From polymers **1** and **2**, we could prepare 70 and 100 nm nanogels at 70 °C, respectively. While the size of the polymer aggregate is reversibly sensitive to temperature, the size of the nanogel formed after the DTT reaction retains the size observed under reaction conditions when it was cooled to room temperature (Figure S2). This result suggests that stable cross-linked nanogels were formed, not polymer aggregates. Using polymer **3**, we could prepare 10 and 26 nm nanogels at 25 and 70 °C, respectively, while the aggregates of polymer **4** were converted to nanogels of 190 nm size at 25 °C. As shown in Figure 3a and b, the hydrodynamic diameter and the autocorrelation function in DLS reveal that fine control over the size of the nanogels can be achieved by controlling the size of the preformed polymer aggregates in water by varying molecular weight, comonomer composition, and temperature. The evidence for the precise size control was further provided by TEM experiments (Figure 3c). TEM images of all nanogels revealed well-defined spherical structures with sizes that correlate very well with the DLS results. These results show that we can systematically tune the nanogel size by controlling the structure of the precursor polymer and by exploiting temperature-dependent aggregation though the LCST behavior of the polymers.

Guest Encapsulation and Triggered/Controlled Release. For a nanocarrier to be effective, it should be able to stably encapsulate lipophilic guest molecules and release its contents in response to a biologically relevant trigger.[20] Disulfide bonds are particularly attractive as stimulus-sensitive functionalities in medicinal chemistry, as they can be cleaved in the presence of high reducing agent concentrations. Reducing agents, such as reduced glutathione (GSH), thioredoxin, and peroxiredoxin, are found at varying levels throughout the body. For example, GSH is found in millimolar concentrations in the cytosol, whereas the extracellular concentration is only micromolar.[21] Therefore, a GSH-sensitive delivery vehicle can be effective in facilitating intracellular delivery of encapsulated molecules.[1g,22]

We hypothesized that GSH could induce release of loaded dyes through cleavage of the disulfide cross-linking bonds and that the release kinetics could be tuned by the cross-linking density in the nanogel. To test this possibility, we prepared three different cross-linked particles by adding 10, 20, or 50 mol % (against the precursor PDS groups) of DTT to polymer **4**. The progress of the reaction was conveniently monitored by release of the pyridothione byproduct through tracing its characteristic absorption at 343 nm. Considering the mechanism by which this addition results in cross-linked polymer particles and the percentage of PDS functionalities in polymer **4**, this reaction should result in nanoparticles **NG1**, **NG2**, and **NG3** with 7%, 14%, and 35% cross-linking densities, respectively, assuming 100% reaction efficiency. Our estimations, based on pyridothione release, indicate that the actual cross-linking densities correspond to 6%, 13%, and 25%, respectively (Figure 4a). DLS studies reveal that the structures obtained are all about 190 nm in size (Figure 4b). TEM images reveal well-defined spherical structures with slightly smaller diameters than those observed in DLS, which is attributed to the possible swelling of the nanoparticles in water (Figure S3). It is interesting to note that the sizes of all three nanogels are very similar. This suggests that the size of the assembly prior to the cross-linking reaction dictates the nanogel size and that further cross-linking occurs within that nanoassembly.

To investigate the possibility of encapsulating hydrophobic guest molecules within the interiors of these nanogels, we carried out the DTT-based cross-linking reaction in the presence of Nile red, a hydrophobic dye. Nile red is inherently insoluble in water. Therefore, the reaction was optimized using acetone as a solvent in the first steps, before addition of water during the cross-linking reaction. Isolation of the nanoparticles and their subsequent dissolution in water retains the presence of Nile red, as discerned by the emission spectra of all three gels (Figure 4c).

To explore triggered release, we added GSH into nanogel solutions and investigated the release of Nile red by tracing the decrease in the hydrophobic dye's spectral emission intensity caused by its insolubility in the aqueous media. To examine the GSH-dependent dye release, Nile red loaded nanogel solutions (0.05 wt %) in pH 7.4 sodium acetate buffer solution were treated with different concentrations of GSH (10 μM and 10 mM), and the intensity of Nile red emission at 610 nm was

(20) (a) Murthy, N.; Thng, Y. X.; Schuck, S.; Xu, M. C.; Fréchet, J. M. J. *J. Am. Chem. Soc.* **2002**, *124*, 12398–12399. (b) Chan, Y.; Wong, T.; Byrne, F.; Kavallaris, M.; Bulmus, V. *Biomacromolecules* **2008**, *9*, 1826–1836. (c) Oh, J. K.; Siegwart, D. J.; Matyjaszewski, K. *Biomacromolecules* **2007**, *8*, 3326–3331. (d) Zhang, L.; Liu, W.; Lin, L.; Chen, D.; Stenzel, M. H. *Biomacromolecules* **2008**, *9*, 3321–3331. (e) Jiang, J.; Qi, B.; Lepage, M.; Zhao, Y. *Macromolecules* **2007**, *40*, 790–792.

(21) (a) Bernkop-Schnürch, A. *Adv. Drug Delivery Rev.* **2005**, *57*, 1569–1582. (b) Sivakumar, S.; Bansal, V.; Cortez., C.; Chong, S.-F.; Zelikin, A. N.; Caruso, F. *Adv. Mater.* **2009**, *21*, 1820–1824. (c) Yang, J.; Chen, H.; Vlahov, I. R.; Cheng, J.-X.; Low, P. S. *Proc. Natl. Acad. Sci. U.S.A.* **2006**, *103*, 13872–13877. (d) Chong, S.-F.; Chandrawati, R.; Städler, B.; Park, J.; Cho, J.; Wang, Y.; Jia, Z.; Bulmus, V.; Davis, T. P.; Zelikin, A. N.; Caruso, F. *Small* **2009**, *5*, 2601–2610.

(22) (a) Jia, Z.; Wong, L.; Davis, T. P.; Bulmus, V. *Biomacromolecules* **2008**, *9*, 3106–3113. (b) Li, Y.; Lokitz, B. S.; Armes, S. P.; McCormick, C. L. *Macromolecules* **2006**, *39*, 2726–2728. (c) Bauhuber, S.; Hozsa, C.; Breunig, M.; Göpferich, A. *Adv. Mater.* **2009**, *21*, 3286–3306. (d) Wu, A. M.; Senter, P. D. *Nat. Biotechnol.* **2005**, *23*, 1137–1146. (e) Bae, K. H.; Mok, H.; Park, T. G. *Biomaterials* **2008**, *29*, 3376–3383. (f) Li, Y.-L.; Zhu, L.; Liu, Z.; Cheng, R.; Meng, F.; Cui, J.-H.; Ji, S.-J.; Zhong, Z. *Angew. Chem., Int. Ed.* **2009**, *48*, 9914–9918.

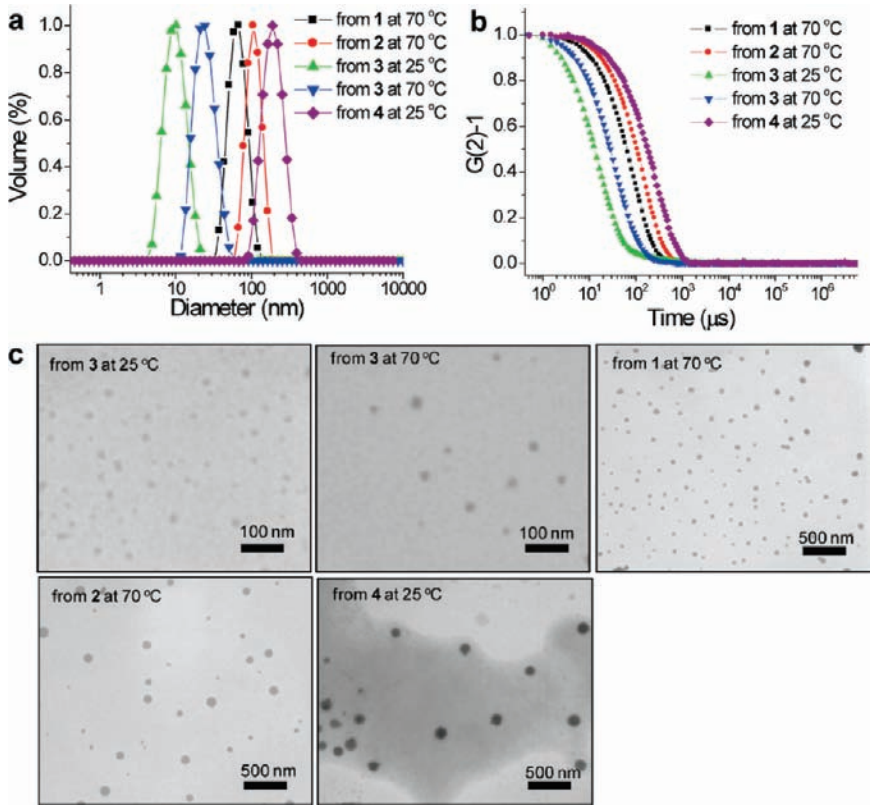

Figure 3. (a) Size distribution of the nanogels prepared by DTT addition into the polymer aggregates at 25 or 70 °C in water and (b) the corresponding autocorrelation functions. (c) TEM images of the nanogels.

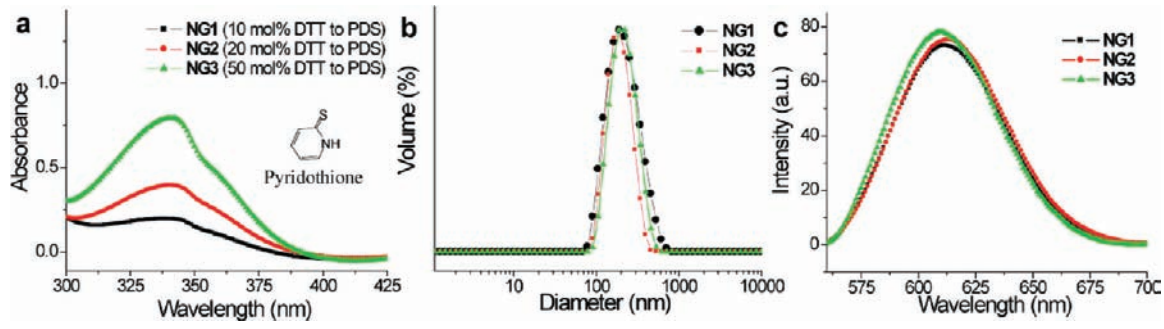

Figure 4. (a) Absorption spectra of pyridothione in UV−vis. Pyridothione, which is a byproduct during nanogel synthesis by disulfide bond formation and shows characteristic absorption at 343 nm wavelength, is monitored in each nanogel (10 mg/mL) prepared. (b) Size distribution of nanogels (1 mg/mL) by DLS. (c) The emission spectra of Nile red sequestered in polymer nanogels.

monitored for three days. At low GSH concentrations (10 μM), little dye release was observed for all nanogels (Figure 5a−c). This concentration corresponds to that commonly observed outside the cell and within the blood plasma. In contrast, high concentrations of GSH (10 mM), corresponding to those found inside the cell, induced significant dye release (Figure 5d−f).

Cross-linking density is most likely to influence the rate of dye release from the nanogel interior. **NG1** (6% cross-linked nanogel) showed rapid release, reaching a plateau after 6 h at 10 mM GSH in pH 7.4 buffer solution. **NG2** (13% cross-linked nanogel) showed slower release, reaching a maximum at 12 h; **NG3** (25% cross-linked nanogel) displayed gradual, highly sustained release for several days. Because the entry of these nanogels would likely involve endocytosis, we were interested in analyzing the release profile at lower pH. We found that the release profile difference under acidic conditions (pH 5) was very similar to that observed with pH 7 (Figure 5g−i and Figure S4). While this bodes well for endocytosis-based entry into the cells, we also found the release profile at high GSH concentration to be surprising, as GSH activity is considered most efficient at neutral pH.[23] As shown in Figure 6, similar release was observed for all three gels over several hours at both pH 5 and 7.4.

Encapsulation Stability and Tunable in Vitro Guest Release. The encapsulation stability of lipophilic molecules is one of the most critical factors of an efficient nanocarrier, preventing significant loss of drug due to leakage during circulation. We have previously developed a fluorescence resonance energy transfer (FRET)-based method to evaluate the encapsulation stability of nanocarriers in aqueous solutions.[11] With this method, we found that the cross-linking densities can

(23) Moskaug, J. O.; Sandvig, K.; Olsnes, S. *J. Biol. Chem.* **1987**, *262*, 10339–10345.

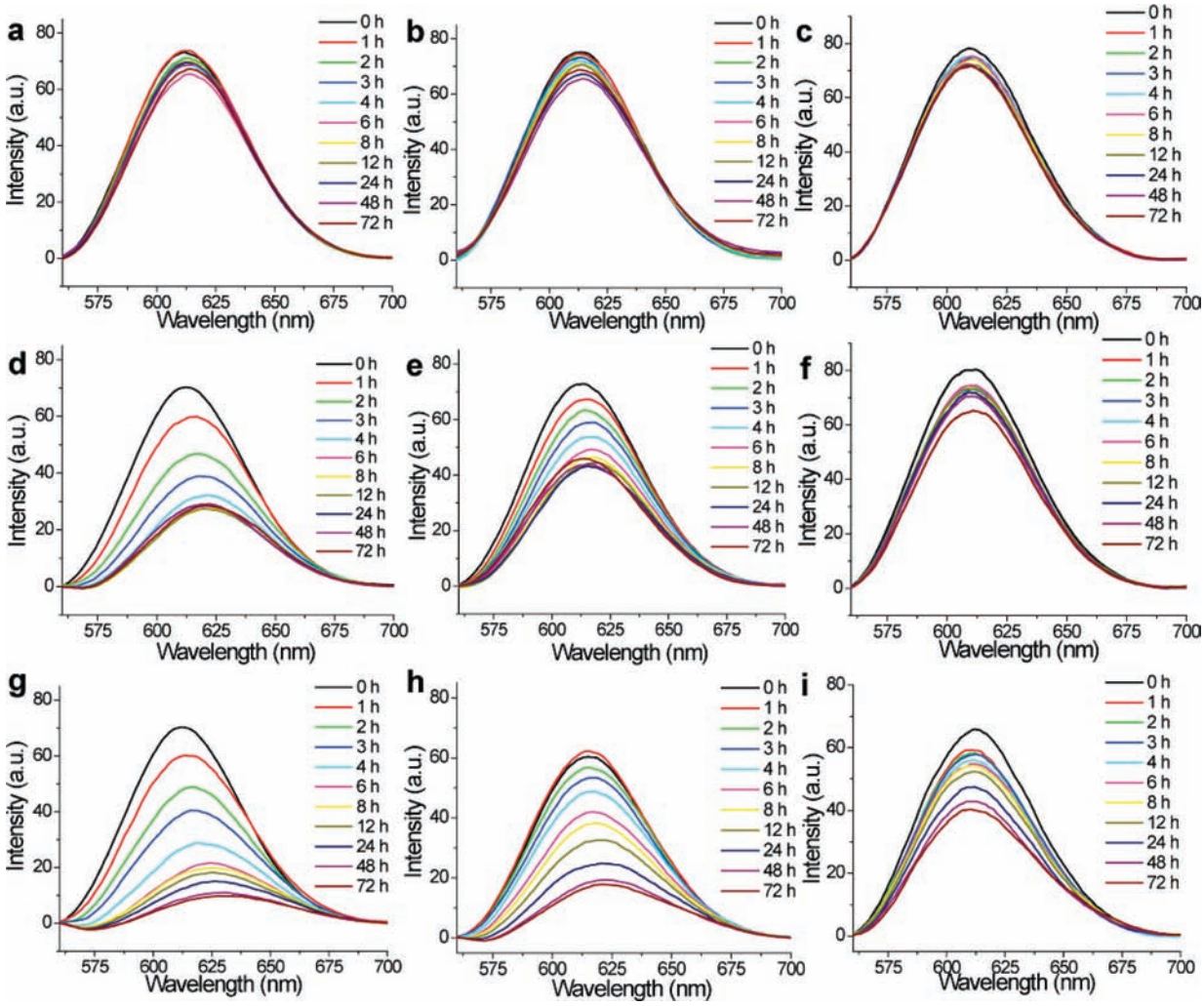

Figure 5. Dye release from the nanogels **NG1** (a,d,g), **NG2** (b,e,f), and **NG3** (c,f,i) (0.05 wt %) in response to varied GSH concentrations. (a−c) 10 μM GSH and (d−f) 10 mM GSH at pH 7.4, and (g−i) 10 mM GSH at pH 5. The release only occurred at high GSH concentration. At acidic pH under 10 mM GSH, the release was faster and more continuous over time than that at neutral pH.

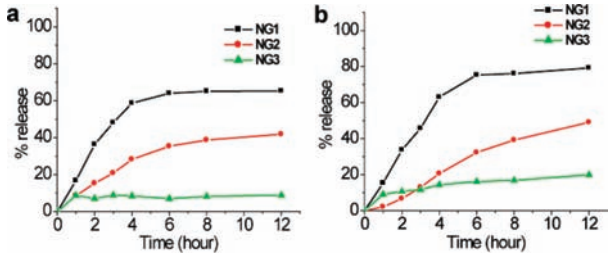

Figure 6. (a) Comparison of GSH-induced dye release rate from the nanogels, which have different cross-linking densities at (a) pH 7.4 and (b) pH 5.

significantly influence the encapsulation stability coefficient (Λ). To correlate with the in vitro guest release experiments, we were also interested in investigating the encapsulation stability of these nanoassemblies in an environment that mimics cells. Accordingly, we carried out FRET experiments to investigate the dye leakage in the presence of dioleoyl phosphatidylcholine (DOPC) bilayer vesicles.[10a] We used FRET between two noncovalently encapsulated dyes as a diagnostic tool (Figure 7a). Nanogel solutions containing a mixture of two hydrophobic dyes, 3,3′-dioctadecyloxacarbocyanine perchlorate (DiO: donor, green fluorescence) and 1,1′-dioctadecyl-3,3,3′,3′-tetramethylindocarbocyanine perchlorate (DiI: acceptor, red fluorescence), were prepared. To confirm that these two dyes exhibit the requisite FRET inside the nanogels, we excited the nanogel solution at 484 nm, the wavelength at which DiO specifically absorbs. We were gratified to note that an intense DiI emission at 575 nm was observed, indicating an efficient energy transfer between the closely packed FRET partners within the nanogel interior (Figure 7b). When this experiment was carried out in acetone, strong DiO fluorescence at 503 nm was observed along with significant reduction of DiI emission, suggesting a loss of FRET due to diffusion of the dyes from the nanogel interior to the solvent. Note that both DiO and DiI are soluble in acetone, but insoluble in water.

It is known that DOPC vesicles can absorb the dye molecules, if available in solution. Therefore, if the dye molecules are not stably encapsulated within the nanogels, the transient presence of these dye molecules in the aqueous milieu will result in equilibration of the dye between the DOPC vesicles and the nanogels. This process will result in loss of FRET with leaky nanogels, due to the sparse distribution of each dye into the bilayer of DOPC. To investigate the behavior of our nanogels, we monitored the fluorescence intensities of nanogel solutions containing DiO and DiI dyes for 3 days by exciting the solution at 484 nm (DiO). The disappearance of FRET due to the release

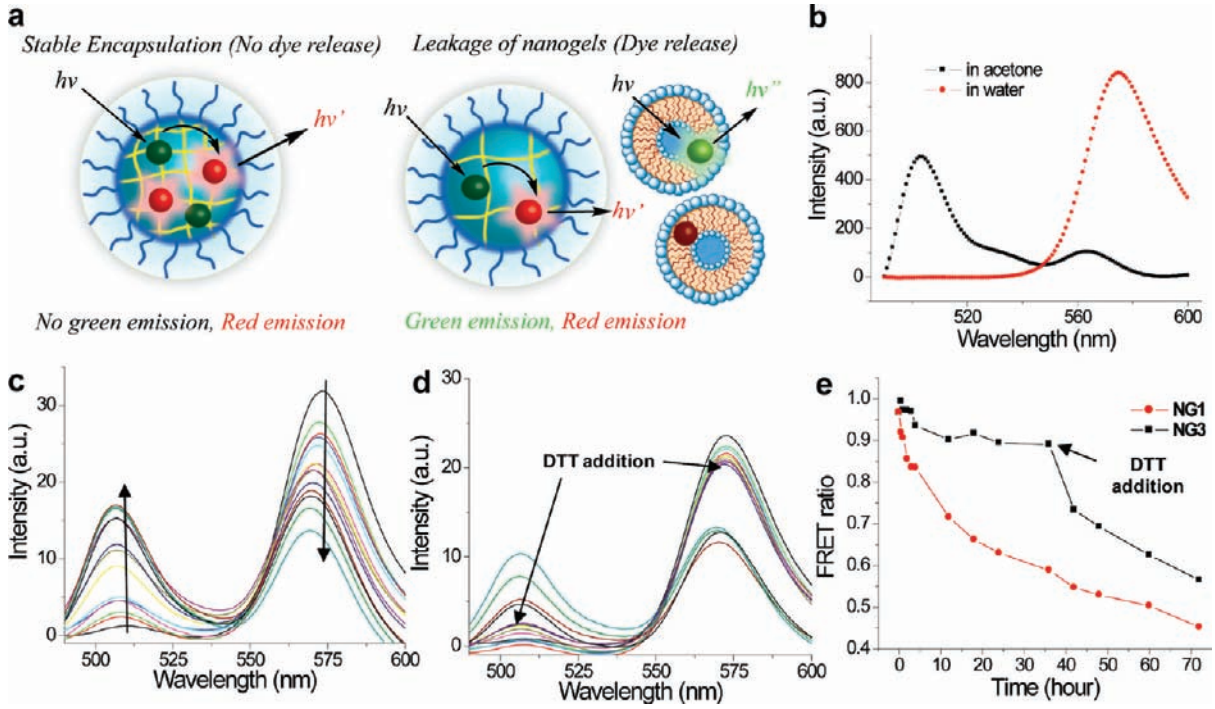

Figure 7. (a) Schematic representation of the stable and leaky nanocontainers identified by a FRET experiment. (b) Fluorescence spectra of nanogels (**NG3**) containing a FRET pair, DiO and DiI. Nanogel solutions (2 mg/mL) were prepared containing two hydrophobic dyes, 1 wt % DiO (donor, fluorescence at 503 nm) and 1 wt % DiI (acceptor, fluorescence at 575 nm). Time-resolved spectra of (c) **NG1** (0.1 mg/mL) and (d) **NG3** (0.1 mg/mL) containing two dyes after mixing with 4 mM DOPC vesicle solution. (e) Change in FRET ratio of the nanogels containing both dyes. The addition of 20 mM DTT to **NG3** after 36 h showed a significant decrease in the FRET ratio.

of hydrophobic guest molecules was then monitored by tracing the increase in the donor (DiO) emission and the concomitant decrease in the acceptor's (DiI). Figures 7c,d shows the change of the dye emission pattern with different cross-linked nanogels, **NG1** (6% cross-linked) and **NG3** (25% cross-linked). In the case of the highly cross-linked nanogel (**NG3**), the emission of FRET remained relatively steady throughout the time of the experiment (Figure 7d), indicating that the two dyes are stably trapped inside the nanogels. Conversely, in the case of the lightly cross-linked nanogel (**NG1**), the acceptor's (DiI) emission gradually decreased over the 3 days period with concurrent increase in the donor's (DiO) emission (Figure 7c). This result indicates that the hydrophobic guest molecules were transferred from the nanocontainer to the DOPC vesicle bilayer. Even though **NG1** showed less encapsulation stability than **NG3**, the leakage is much slower than that from block copolymer micelles previously reported,[10a] suggesting the versatility of these nanogels as a delivery vehicle candidate. The addition of DTT (20 mM) to the stable nanocontainer (**NG3**) containing the two dyes led to decreasing FRET (Figure 7d). The FRET ratio $I_a/(I_d + I_a)$ plotted against time, where I_a and I_d are the maximum emission intensities of the acceptor (DiI) and the donor (DiO) at 575 and 503 nm, respectively, clearly shows the difference in encapsulation stabilities of these nanogels (Figure 7e). This result means that the drug molecules can stably stay inside the nanocontainer during circulation, but be released inside the target cells in response to the higher reductant (GSH) levels.

Next, we were interested in testing the in vitro release of guest molecules. Here, we again utilized nanogels having DiO and DiI coencapsulated within their interiors. In this case, if there were no guest release upon cellular internalization, then FRET would be continually observed within the cytosolic interior. However, if the guest release did occur, then the proximity between the DiO and DiI would greatly increase, causing a qualitative decrease in FRET observation. Thus, the distribution of red (FRET, 585−615 nm spectral filter) and green (no FRET, 505−520 nm spectral filter) fluorescence was observed over time by confocal microscopy (λ_{ex} = 488 nm). Figure 8 shows the fluorescence microscopy images of our study. After 2 h, neither of the nanogels had gained significant access to the cells (Figure 8a and d). Most of the red fluorescence was found in the extracellular environment. The observed red fluorescence suggests that the dye molecules are still intact in the polymer nanoparticles. In the case of **NG1** (6% cross-linked), green color begins to appear in the cell membrane with a little red color inside the cell after an incubation period of 4 h (Figure 8b). The green fluorescence (DiO) in the plasma membrane suggests an initial loss of FRET due to hydrophobic dye transfer from the nanogels to the membrane. As time progresses, the extent of fluorescence (both green and red) increases; the observed yellow color is essentially an overlay of the two colors. After accessing the cell, the green fluorescence from DiO and the red fluorescence from DiI appear more equally inside the cells. This indicates that there is a significant release of the dye molecules from the nanogel, because there is no energy transfer that causes the green fluorescence to be suppressed. While the lightly cross-linked gel, **NG1**, shows initial dye release from the nanogels to plasma membrane before cellular internalization, the highly cross-linked **NG3** exhibits complete internalization prior to any significant release. This difference is clearly observed in Figure 8e, which shows an abundance of red color and a little yellow color inside the cell with no green color at the membrane after 4 h incubation. At 24 h incubation, the intensity of yellow color increased, but the dominant red color indicates slower release due to the dense cross-linking (Figure 8f). However, after 48 h

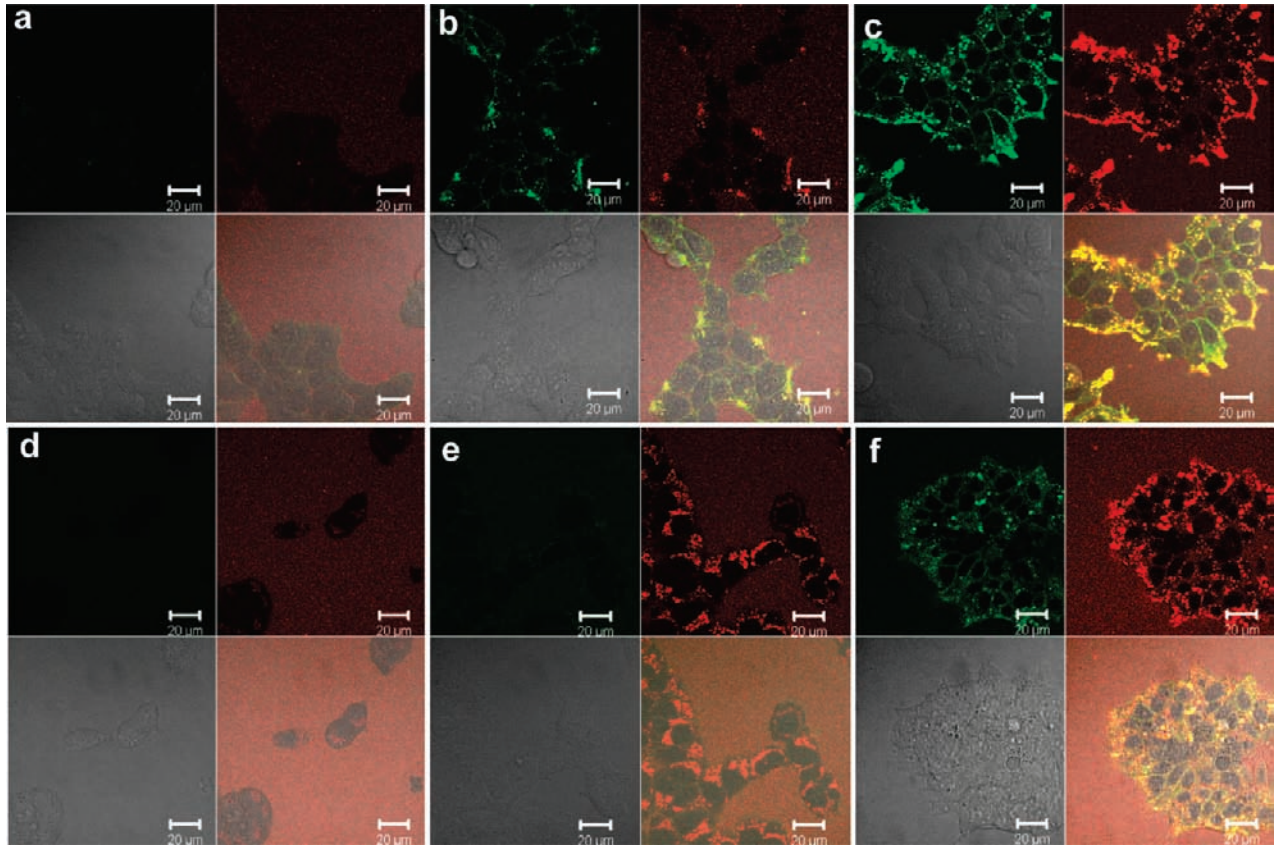

Figure 8. Confocal microscopy images of nanogels containing DiO and DiI as a FRET pair at different incubation times. **NG1**, 6% cross-linked gels, were incubated with MCF-7 cells for (a) 2 h, (b) 4 h, and (c) 24 h. **NG3**, 25% cross-linked gels, were incubated with MCF-7 cells for (d) 2 h, (e) 4 h, and (f) 24 h. Within each image set, top left is the DiO channel that shows green color (no FRET, dye release), and top right is the DiI channel that shows red color (FRET, no dye release). Bottom left is the DIC image, and bottom right is an overlap of all three. Yellow color is overlay of green and red. Scale bar is 20 μm.

of incubation, yellow color dominates the image, implying the progression of nanogel disruption and subsequent dye release (Figure S5).

After entry, the less cross-linked nanoparticle **NG1** releases the dye molecules faster than the more cross-linked **NG3**. It is evident from Figure 8 that the difference between the green and the red fluorescence from these cells is much smaller in the case of **NG1**, as compared to **NG3**. These results suggest that the intracellular GSH acts on **NG1** faster than **NG3**, just as observed with our Nile red release studies outlined above, and are consistent with the dye release differences depending on cross-linking density from the nanogels to the DOPC bilayer. For efficient drug delivery, it is desirable that drugs be stably entrapped inside the vehicle before reaching a target cell and then are released in response to an intracellular trigger. These features are indeed present in our polymer nanogel. More importantly, our results here are a demonstration of the tunability in stability of encapsulation and guest release in cells. The entry of our nanoparticles into the cells seems slow in these in vitro experiments. However, it is noteworthy that these processes can be accelerated using ligands that facilitate internalization by recognizing cell surface receptors. We have demonstrated this possibility by decorating these nanogels with a cell-penetrating peptide in our preliminary communcation.[12]

Intracellular Delivery of Doxorubicin. Considering the results that we obtained through in vitro dye release, we were interested in testing the translation of this work to chemotherapeutic delivery. Thus, we have carried out in vitro cell viability assays for these polymer nanoparticles. We anticipated that our gels would be relatively nontoxic, as they are composed of biocompatible OEG units as surface displays in a methacrylate backbone. Cell viability was investigated by treating 293T human kidney cell lines with nanogels. 293T cells were treated with different concentrations of nanogel solutions and were incubated for 24 h. Cell viability was measured using the Alamar Blue assay. As shown in Figure 9a, the nanogels exhibit high cell viability and no concentration-dependent toxicity up to a nanogel concentration of 1 mg/mL. This result indicates that the nanogel material is nontoxic and thus a potential candidate for biological applications.

To investigate the possibility of utilizing these polymer nanoparticles as drug delivery vehicles, we encapsulated the chemotherapeutic cytotoxic drug molecule, doxorubicin (Dox), during nanogel synthesis by in situ loading. The loading capacities were found to be 24 and 20 wt % for **NG1** and **NG3**, respectively. The Dox-loaded nanogels were added to MCF-7 cells, and the extent of cell death was investigated after 72 h. As shown in Figure 9b, the Dox-loaded nanoparticles were toxic, but exhibited slightly lower toxicities than the free drug. This is presumably caused by the delayed release of Dox from the nanogels inside the cells, while free Dox molecules easily diffuse through the cellular membrane. As compared to small drug molecules, however, the nanogels are likely to be more efficient in vivo because of the passive targeting of the nanosized particles to tumor tissue by the enhanced permeability and retention effect. Interestingly, both **NG1** and **NG3** containing

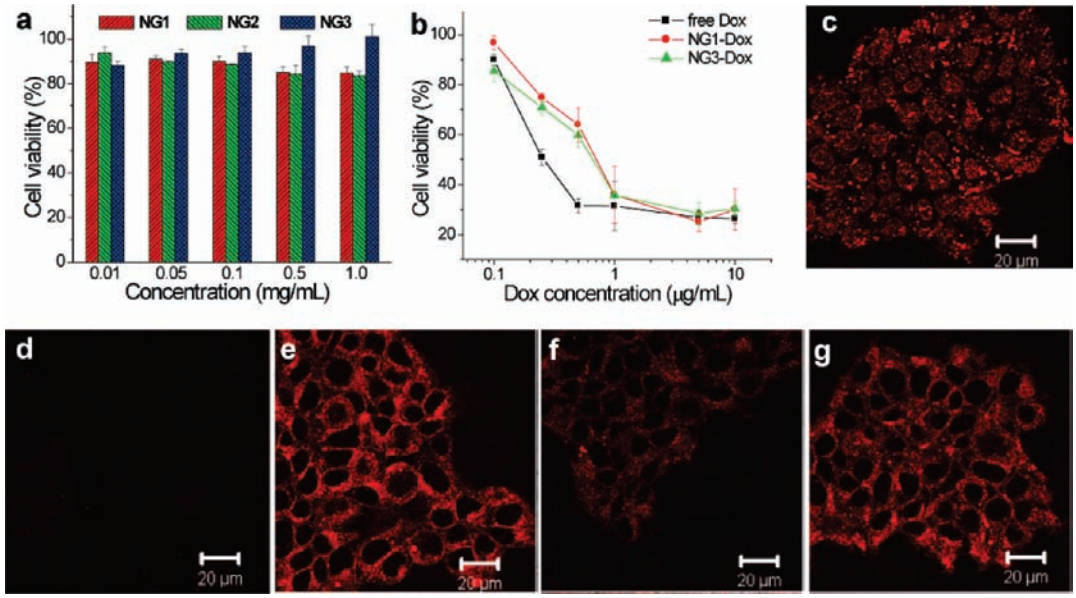

Figure 9. (a) In vitro toxicity of empty nanogels with 293T cells after 24 h incubation; (b) Dox-loaded nanogels with MCF-7 cells after 72 h incubation; and confocal microscopy images of (c) free-Dox after 3 h; **NG1-Dox** after (d) 3 h and (e) 4 h; and **NG3-Dox** after (f) 3 h and (g) 4 h.

Dox showed similar toxicity. This is quite different from what we expected. We expected that **NG1-Dox** would be more toxic than **NG3-Dox** because, as described above, the lightly cross-linked **NG1** showed faster dye release in the cell as well as in buffer solution. One possible explanation is a difference in the cellular uptake between the nanoparticles of different cross-linking densities.[24] We previously observed uptake differences by in situ dye release experiments. As shown in Figure 8b and e, **NG3** exhibited higher cellular uptake relative to **NG1** at the same time period.

For further study, we monitored the cell uptake of both free Dox and Dox-loaded nanogels (20 μM Dox concentration) using confocal microscopy over time. Initial internalization of Dox was observed within 3 h for free Dox and **NG3-Dox**, but not until 4 h for **NG1-Dox** (Figure 9c−g). While the free Dox showed significant accumulation in the nucleus after 3 h (Figure 9c), **NG1-Dox** and **NG3-Dox** only showed strong fluorescence in the cytoplasm (Figure 9e−g). Even though **NG1** exhibited faster dye release in previous experiments, the effective Dox amount released from **NG3** might be similar to that from **NG1** due to the differences in cellular uptake. This is presumably the reason that the two nanogels show similar toxicities. The reason for the faster uptake of **NG3** is not clear to us at this time. It should be noted that the question of optimal cross-linking density for in vivo drug delivery remains unanswered because of many unknown factors in the body and will be studied, in detail, in our future in vivo studies.

Conclusions

Biocompatible nanogels that are able to encapsulate hydrophobic drug molecules in situ were synthesized using intra-/intermolecular disulfide cross-linking with PDS containing polymers. As the nanogel is formed by the cross-linking of PDS functionalities and because the nanogel size is directly determined by the size of the polymer aggregate in water, the nanogel sizes have been effectively controlled from 10 to 200 nm by varying the molecular weight, temperature, and the relative ratio of comonomers in the polymers. By varying the cross-linking density of the nanogels, the stability of encapsulation can be tuned and the release kinetics of guest molecules can be controlled. We show that the noncovalently encapsulated dye molecules can be released in response to a redox trigger, glutathione (GSH), because the cross-linking disulfide bonds are degradable in a reducing environment. Stability of dye encapsulation inside the nanogels and tunability in the release of the guest molecules have been demonstrated through in vitro fluorescence resonance energy transfer (FRET) experiments. Additionally, we have utilized these polymeric nanoparticles to sequester hydrophobic chemotherapeutic drug molecules and release them intracellularly to achieve drug-induced cytotoxicity. Overall, these nanogels exhibit significant stability, allowing for tunable controlled release after cellular penetration. Additionally, these vehicles do not seem to suffer from loss of guest molecules prior to cellular entry. Because the formation of the reversible nanogels and subsequent loading of guest molecules are quite simple and produce containers with high encapsulation stabilities and tunable release kinetics, this polymer nanogel scaffold holds great potential for drug delivery, especially for chemotherapeutics. Future work will be devoted to detailed study of in vivo delivery with selective ligands for targeting specific cell types.

Acknowledgment. This work was supported by DARPA and the NSF-MRSEC.

Supporting Information Available: Experimental details. This material is available free of charge via the Internet at http://pubs.acs.org.

JA1069932

(24) (a) You, J.-O.; Auguste, D. T. *Nano Lett.* **2009**, *9*, 4467–4473. (b) Beningo, K. A.; Wang, Y.-l. *J. Cell Sci.* **2002**, *115*, 849–856.